DYNAMICAL DECOUPLING OF NESTED BARS: SELF-GRAVITATING GASEOUS NUCLEAR BARS

Peter Englmaier
Astronomisches Institut, Universität Basel, Venisstrasse 7, CH-4102, Binningen, Switzerland
email: Peter.Englmaier@unibas.ch
and

Isaac Shlosman
Department of Physics and Astronomy, University of Kentucky, Lexington, KY 40506-0055, USA
email: shlosman@pa.uky.edu

ABSTRACT

A substantial fraction of barred galaxies host additional nuclear bars which tumble with pattern speeds exceeding those of the large-scale (primary) stellar bars. We have investigated the mechanism of formation and dynamical decoupling in such nested bars which include gaseous (secondary) nuclear bars within the full size galactic disks, hosting a double inner Lindblad resonance. Becoming increasingly massive and self-gravitating, the nuclear bars lose internal (circulation) angular momentum to the primary bars and increase their strength. Developing chaos within these bars triggers a rapid gas collapse — bar contraction. During this time period, the secondary bar pattern speed $\Omega_{\rm s} \sim a^{-1}$, where a stands for the bar size. As a result, $\Omega_{\rm s}$ increases dramatically until a new equilibrium is reached (if at all), while the gas specific angular momentum decreases — demonstrating the dynamical decoupling of nested bars. Viscosity, and therefore the gas presence, appears to be a necessary condition for the prograde decoupling of nested bars. This process maintains an inflow rate of ~ 1 M$_\odot$ yr^{-1} over $\sim 10^8$ yrs across the central 200 pc and has important implications for fueling the nuclear starbursts and AGN.

Subject headings: hydrodynamics — galaxies: active — galaxies: evolution — galaxies: kinematics and dynamics — galaxies: spiral — galaxies: starburst

1. Introduction

A large fraction, $\sim 1/3$, of barred galaxies host a secondary (nuclear) bar in the central regions, in addition to the primary, large-scale stellar bar (Laine et al. 2002; Erwin & Sparke 2002). Ironically, such nested bar systems have been predicted theoretically, including their most intriguing property — the state of dynamical decoupling (Shlosman, Frank & Begelman 1989; Shlosman, Begelman & Frank 1990). Few examples of double barred galaxies have been observed already in the 1970s, but have been classified as having triaxial (elliptical) bulges rather than nuclear bars (de Vaucouleurs 1974; Sandage & Brucato 1979; Kormendy 1982). Both stellar and mixed type bars (e.g., Buta & Crocker 1993; Shaw et al. 1995; Friedli et al. 1996; Jungwiert, Combes & Axon 1997; Jogee, Kenney & Smith 1998; Knapen, Shlosman & Peletier 2000), as well as gaseous nuclear bars (e.g., Ishizuki et al. 1990; Devereux, Kenney & Young 1992; Forbes et al. 1994; Mirabel et al. 1999; Kotilainen et al. 2000; Maiolino et al. 2000) have been detected. Random mutual orientation of the observed nested bars confirms that they spend a substantial fraction of their lifetime in the decoupled state — tumbling with different pattern speeds.

Numerical simulations have shown indeed that

pattern speeds of the mixed nuclear bars are substantially larger than those of the primary stellar bars (e.g., Friedli & Martinet 1993: Combes 1994; Heller & Shlosman 1994). However, purely stellar nuclear bars form only under special initial conditions (e.g., Friedli & Martinet 1993), while gaseous bars have been claimed not to decouple (Wada & Habe 1992; Combes 1994). A number of issues have never been resolved — what triggers the dynamical decoupling of nested bars? Do purely gaseous self-gravitating bars form, and can they decouple from the primary bars? In this Letter we use numerical simulations of self-gravitating gas in galactic disks to show that gaseous bars form and decouple as a result of stellar bar-driven inflow into the central kpc. Furthermore, we study the physical reasons for this dynamical runaway in nested bar systems (see also Shlosman 2003; and in preparation).

2. Numerical Modeling

Cold gas forms a thin layer in disk galaxies. Because we are basically interested in the dynamical evolution of this layer, we limit the simulations to the disk midplane and use the updated 2-D version of our Smoothed Particle Hydrodynamics (SPH) code (e.g., Heller & Shlosman 1994). For test purposes we also make use of the grid code ZEUS-2D (Stone & Norman 1992). The initial conditions have been tailored in order to focus on the role of central resonances in disk galaxies by modifying the background analytical potential of Miyamoto & Nagai (1975), $\Phi(r) = -GM/\sqrt{r^2 + A^2}$, using prescription from Englmaier & Shlosman (2000). Here M is the mass of a halo, bulge or a disk, and A is the radial lengthscale, all given in Table 1, and r is the radius vector in the disk plane. Adjustments to this potential allow us to specify the positions of axisymmetric resonances: the inner inner and outer inner Lindblad resonances (IILR, OILR) and the corotation. Positions of these resonances correspond to the solutions of equation $\Omega - \kappa/2 = \Omega_{\rm p}$, where Ω, κ and $\Omega_{\rm p}$ are angular velocity, epicyclic frequency and primary bar pattern speed. For the models presented here, those are fixed at $r = 0.5$ kpc, 2 kpc and 6 kpc respectively. The primary stellar bar is given by the Ferrers' (1877) potential with $n = 1$ and rotates with a prescribed pattern speed $\Omega_{\rm p} = 25.46$ Gyr^{-1}. Its mass, the semi-major (a) and semi-minor (b) axes are 4×10^9 M$_\odot$, 5 kpc and 1.25 kpc, respectively. The axisymmetric contribution from the primary bar mass is included in the initial conditions. The non-axisymmetric part is brought up gradually in order to avoid transients. The number of SPH particles has been varied between $N = 10^4$ and 4×10^5 and the minimal gravitational softening has been fixed at 150 pc. A large number of models have been run with increasing gas contents. Here we only discuss a representative model showing a nested bar descoupling, with the gas mass 5×10^8 M$_\odot$ within the corotation, which corresponds to $\sim 2.7\%$ of the total mass within 3 kpc — the initial radial scalelength of the isothermal gas. The gas sound speed is 10 km s^{-1}.

Table 1: Model Parameters

Component	Mass (10^{10} M$_\odot$)	A (kpc)
halo	5	9
bulge	0.4	0.2
disk	2	3
gas	0.05	3

3. Results

As the large-scale bar is brought up gradually, the gas within the corotation radius forms a pair of trailing offset shocks and falls inwards losing its angular momentum via gravitational torques induced by the primary bar (see Fig. 1 and Animation Sequence 1). At around $\sim$ 1 kpc, the shocks curve azimuthally, and the gas flow is shock-focused into more circular orbits attempting to form an ovally-shaped nuclear ring. The gas inside the central kpc is losing its angular momentum forming a secondary bar which leads the primary bar by a constant angle $\sim 50^\circ - 60^\circ$ and a pattern speed $\Omega_{\rm s} = \Omega_{\rm p}$, and has a flat density distribution. A pair of leading shocks form between this nuclear bar and the ring. Almost immediately the ring fragments and gradually merges with the nuclear bar. At around $t \sim 0.35 - 0.4$ Gyr this secondary bar with a semimajor axis of 1 kpc and ellipticity $\epsilon \sim 0.65$ decouples in the *retrograde* direction, in the primary bar frame (still prograde in the inertial frame). One can follow up the subsequent evolution in one of the three frames of reference: inertial, primary or secondary. We mostly employ the first two.

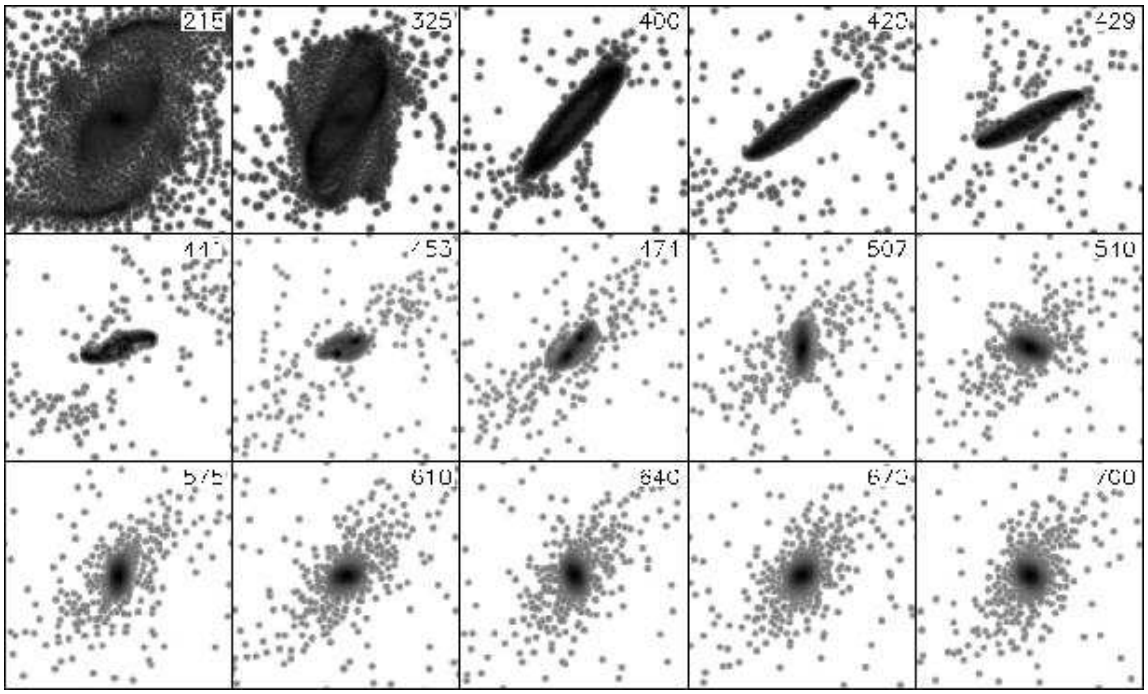

Fig. 1.— Gas evolution in the central 3 kpc×3 kpc part of a barred galaxy in the frame of the primary bar (Animation Seq. 1). Rotation is anti-clockwise and the primary bar is horizontal. The time in Myrs is shown in the right upper corners (see text for more details).

This unusual behavior of the gaseous bar is a result of gravitational torques from the primary bar (Heller, Shlosman & Englmaier 2001; see also below). Its swing towards the position angle of the primary bar is accompanied by a loss of internal (i.e., circulation) and precession (tumbling) angular momenta in the gas. The bar ellipticity increases to ~ 0.85 (Fig. 2) and $\Omega_{\rm s}$ drops to ~ 12 Gyr^{-1} (Fig. 3) in the inertial frame. Next, the gaseous bar reverses its tumbling to the *prograde* one (in the primary frame) and quickly shrinks to much smaller radii. This reversal coincides with a dramatic gas inflow (Fig. 4). The gas density distribution in the secondary bar becomes centrally peaked. The avalanche inflow clearly leads to a period of an unstable bar shape, ~ 0.1 Gyr long. The bar apparently fragments during the collapse and two fragments preserve their identity and store some of the circulation angular momentum during this time (e.g., $t = 0.474$ Gyr in Fig. 1). The final value of $\Omega_{\rm s} \sim 85$ Gyr^{-1} is achieved at $t \sim 0.6$ Gyr with some superposed bar length oscillations which are well correlated with the mutual orientation of both bars.

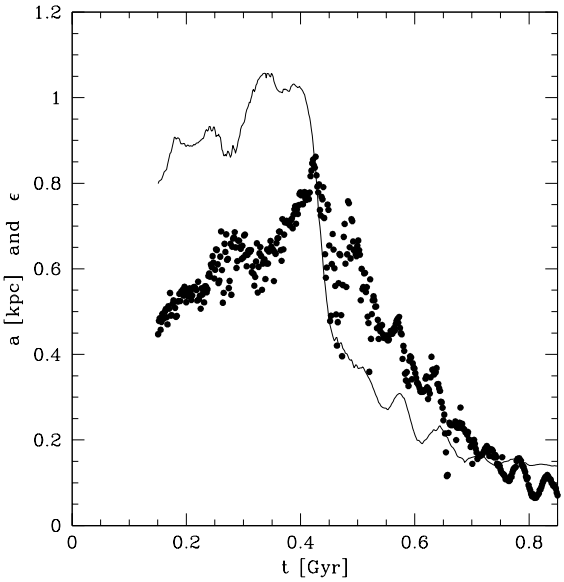

Fig. 2.— Evolution of ellipticity, $\epsilon = 1 - b/a$ (dotted line), and semimajor axis, a (solid line) of the secondary bar.

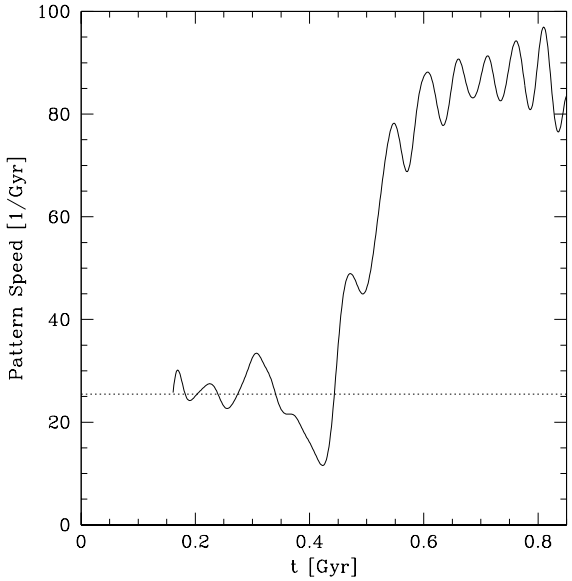

Fig. 3.— Pattern speeds of primary ($\Omega_{\rm p}$, dotted line) and secondary ($\Omega_{\rm s}$, solid line) bars in the inertial frame.

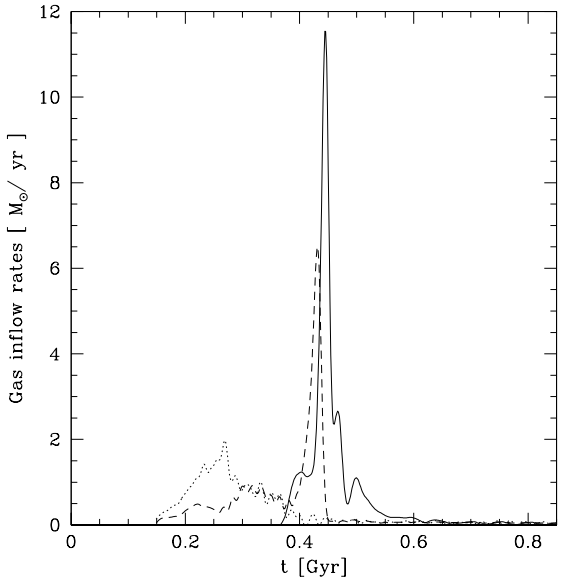

Fig. 4.— Evolution of gas inflow rates across the central 175 pc (solid line), 600 pc (dashed line) and 1 kpc (dotted line). The peak at 0.45 Gyr is unresolved.

The observed pattern speed reversal (i.e., speedup in the inertial frame) represents the dynamical runaway (decoupling) of the gaseous bar from the primary bar. The secondary pattern speed has first decreased from $\Omega_{\rm s} = \Omega_{\rm p}$ to its minimal value of ~ 12 Gyr^{-1} and then increased to the maximal ~ 85 Gyr^{-1} $\sim 3.4\Omega_{\rm p}$ where it has stabilized (Fig. 3). By $t \sim 0.7$ Gyr the bar has shrank to ~ 150 pc. This final bar size is the result of a limiting gravitational softening (Section 2). Fig. 4 shows the gas mass inflow rates across a number of characteristic radii. The time delays between the peak rates confirm that the avalanche inflow propagates from larger to smaller spatial scales. The mass ratio of secondary-to-primary bar, f, toward the end of this evolution is ~ 0.1, and the gaseous bar contains about 16% of the total mass within its radius.

Next, we analyze this gas evolution and address the focal questions — what exactly triggers the secondary bar decoupling process and what determines the final secondary pattern speed. We only focus on the essential details here. Some of the observed features in this model do not seem to be of a principal importance. For example, the retrograde swing of the gaseous bar, although is interesting and maybe relevant in some systems, is not crucial for the subsequent prograde decoupling as other models show (in preparation). On the other hand, we find that changes in the gas density and bar size lead directly to the increase in the central mass concentration in the bar, thus amplifying the self-gravitational effects in the gas, affecting dynamics of the system, and triggering the observed runaway.

First, when the secondary bar forms, it extends to the radius of the Max$(\Omega - \kappa/2)$ curve, at ~ 1 kpc. This is also the radius where the nuclear ring attempts to form. The radial density profile in the gaseous bar is flat and even centrally depressed, because the IILR not only prevents the gas inflow to within 500 pc of the center, but also applies torques which expell some of the gas across the IILR. The gas response between the ILRs is $\sim 50 - 60^\circ$ out of phase with the primary bar[1] defining the initial position angle of the secondary bar. The Jacobi energies, $E_{\rm J}$ (e.g., Binney & Tremaine 1987), of the gas are distributed around the IILR as a Gaussian with $\Delta E_{\rm J}/E_{\rm J} \sim 5\% - 10\%$

[1]The so-called periodic x_2 orbits in the notation of Contopoulos & Papayannopoulos (1980) are oriented at 90° to the bar and serve as attractors for the gas motion. The viscous torques prevent the gas response from being completely aligned with the x_2 orbits

(e.g., Fig. 4 of Heller et al. 2001).

Second, two important developments accompany this evolution: the gaseous bar mass increases due to the continuous inflow, and the specific *internal* angular momentum (i.e., circulation) in the bar decreases due to the ongoing torquing from the primary bar (note that the secondary bar is positioned in the first and third quadrants). Loss of internal circulation increases the bar ellipticity by diminishing its minor axis, thus forcing the gas inwards across the IILR (i.e., as measured by $E_{\rm J}$ distribution of gas particles). When $\sim 50\%$ of the gas mass crosses the IILR, it does not find any supporting periodic orbits — these are aligned with the primary bar inside the IILR. The primary bar then torques the gas, which, because it leads the bar by less than 90°, swings in the retrograde fashion towards the main bar. Fig. 3 clearly displays this $\Omega_{\rm s}$ slowdown in the inertial frame.

Third, increasing ϵ (i.e., bar strength) to $\gtrsim 0.8$ in the stellar bars generates a substantial chaos (e.g., Udry & Pfenniger 1988; Martinez-Valpuesta & Shlosman 2004) — the self-gravity is necessary for this. For a gaseous bar, this leads to a shock dissipation and to a dramatic gas inflow. El-Zant & Shlosman (2003) have studied the stability of nested bar systems using the Liapunov exponents and find that this system has a narrow "window" for a stable co-existence — otherwise a mutually excited chaos develops. If $f \lesssim 0.01$, the secondary bars cannot exist in the decoupled phase as no orbits aligned with these bars have been found. On the other hand, when $f \gtrsim 0.15$, the primary bar becomes increasingly chaotic at the bar-bar interface. The value $f \sim 0.1$ obtained here fits comfortably within the allowed range.

The main effect of intrinsic dissipation is the sudden increase in the central mass concentration and in the gas self-gravity. This is nicely exhibited by the radius of $\mathrm{Max}(\Omega - \kappa/2)$ which is dragged inwards by the collapsing gas from ~ 1 kpc. In fact, the secondary bar length follows exactly this radius, which represents the position of the ILRs to a large degree. This is not surprising, as these resonances are main generators of chaos in disk galaxies. Because the gas cannot reside on intersecting orbits, gaseous bars are expected to be limited in size to within their ILRs, if the latter exist.

Although the gas in the model contributes only $\sim 2\%$ of the total mass within the primary bar corotation at 6 kpc, it alters substantially the position of the IILR at later times, as the gas fraction of the total mass within the secondary bar radius ends up at $\sim 16\%$. This is verified through the appearance of a characteristic orbital family in the nonlinear orbit diagram (in preparation), but even the linear (epicyclic) diagrams exhibit this clearly.

Overall, the gaseous bar shrinks by a factor of ~ 7 from the decoupling moment and its pattern speed $\Omega_{\rm s}$ increases by the same amount (Figs. 2, 3). Their product, $\Omega_{\rm s} a \sim const.$, varies by $\pm 22\%$ only. This corresponds to a decrease in the tumbling angular momentum of the bar, $\sim \Omega_{\rm s} a^2$, by a factor of ~ 7. Qualitatively this means that the gaseous bar is speeding up when contracting, and is losing some of its angular momentum to the primary bar torques. To verify that this effect is driven by the gas self-gravity, we have evolved the same model neglecting the gas gravity. The evolution diverges at the retrograde swing — the non-self-gravitating bars do not generate additional chaos and dissipation, and do not decouple in the prograde direction. Requirement for dissipation underscores that a sufficient viscosity, and, therefore, a presence of the gas is a necessary condition for prograde decoupling of nested bars.

We note, that approximate constancy of $\Omega_{\rm s} a$ for the decoupling bar discussed above has some analogy with the secular evolution of stellar bars. Those are known to extend to their corotation (e.g., Athanassoula 1992). Because the corotation radius typically lies in the flat part of the galactic rotation curve and so $\Omega \sim r^{-1}$, this leads $\Omega_p a \sim const.$ One can show that the same relation can be worked out in the epicyclic approximation for decoupling gaseous bars as well, on the assumption that their size is limited by the radius of the IILR — which is supported by our simulations.

An interesting question is to what degree both bars in the decoupled phase exchange energies via mechanism known as a mode coupling (e.g., Sygnet et al. 1988; Massett & Tagger 1997). The corotation radius corresponding to the final $\Omega_{\rm s}$ is positioned close enough to the OILR of the primary bar, and their nonlinear interaction here is not out of question. However, mode coupling does not seem to contribute to the nested bar decoupling itself. It can of course play an important role in locking these two modes in the resonance interaction when both bars are fully developed.

This issue will be addressed elsewhere.

We note two more comments. First, the initial retrograde (in the frame of the primary bar) swing of the secondary bar does not seem to be of a principal importance. When the gas mass is increased just by 20%, the bar decouples directly into the prograde direction. Second, the model gaseous bar is expectedly triggered by the primary bar. In the control run with the same mass distribution but without the non-axisymmetric contribution from the large-scale bar, the nuclear bar did not develop and the central kpc remained nearly axisymmetric.

In summary, in a fully developed galactic disk with a double ILR, a secondary gaseous bar forms in response to the gas inflow along the stellar bar. Initially corotating with the primary bar, this gaseous bar extends to radii where nuclear rings are known to form. Subsequent mass inflow and loss of circulation angular momentum to the stellar bar via gravitational torques strengthens this bar — a process which leads to development of chaotic orbits within the bar and, unlike in purely stellar bars, to a rapid gas infall of ~ 1 $M_\odot$ yr^{-1} over $\sim 10^8$ yrs across the central 200 pc, as gas cannot populate intersecting orbits. As the bar pattern speed appears to be inversely proportional to bar's shrinking size, the pattern speed increases manyfold, triggering a runaway dynamical decoupling of the gaseous bar from the stellar bar. The gaseous bars extend only to their ILRs, unlike their stellar counterparts. Although numerical simulations of this avalanche inflow necesarily are limited by a finite dynamic range which cuts off the inflow, it can in principle proceed to much smaller scales and has implications for fueling nuclear starbursts and AGN. The outcome of this process depends on a number of physical processes which are not included in numerical simulations here, such as a runaway star formation and the degree of clumpiness of the interstellar matter.

We thank Amr El-Zant, Ingo Berentzen, Clayton Heller and Barbara Pichardo for fruitful discussions, technical assistance and comments on manuscript. I.S. is partially supported by NASA/ATP/LTSA grants NAG5-10823, 5-13063, by NSF AST-0206251, and by HST AR-09546 and 10284 from STScI, which is operated by AURA for NASA, under NAS5-26555.

REFERENCES

Athanassoula, E. 1992, MNRAS, 259, 345

Binney, J. & Tremaine, S. 1987, Galactic Dynamics (Princeton Univ. Press)

Buta, R., Crocker, D. 1993, AJ, 105, 1344

Combes, F., Gerin, A. 1985, A&A, 150, 327

Combes, F. 1994, in *Mass-Transfer Induced Activity in Galaxies,* ed. I. Shlosman (Cambridge Univ. Press), 170

Contopoulos, G., Papayannopoulos, T. 1980, A&A, 92, 33

de Vaucouleurs, G. 1974, in IAU Symp. 58, The Formation and Dynamics of Galaxies, ed. J.R. Shakeshaft (Dordrecht: Reidel), 335

Devereux, N.A., Kenney, J.D., Young, J.S. 1992, AJ, 103, 784

El-Zant, A., Shlosman, I. 2003, ApJ, 595, L41

Englmaier, P., Shlosman, I. 2000, ApJ, 528, 677

Erwin, P., Sparke, L.S. 2002, AJ, 124, 65

Ferrers, N.M. 1877, Q.J. Pure Appl. Math., 14, 1

Forbes, D.A., Kotilainen, J.K., Moorwood, A.F.M. 1994, ApJ, 433, L13

Friedli, D., Martinet, L. 1993, A&A, 277, 2

Friedli, D., Wozniak, H., Rieke, M., Martinet, L., Bratschi, P. 1996, A&AS, 118, 461

Heller, C.H., Shlosman, I. 1994, ApJ, 424, 84

Heller, C.H., Shlosman, I. 1996, ApJ, 471, 143

Heller, C.H., Shlosman, I., Englmaier, P. 2001, ApJ, 553, 661

Ishizuki, S., Kawabe, R., Ishiguro, M. Okumura, S. K., Morita, K.-I. 1990, Nature, 344, 224

Jogee, S., Kenney, J.D.P., Smith, B.J. 1998, ApJ, 494, L185

Jungwiert, B., Combes, F., Axon, D.J. 1997, A&AS, 125, 479

Knapen, J.H., Beckman, J.E., Heller, C.H., Shlosman, I., de Jong, R.S. 1995a, ApJ, 454, 623

Knapen, J.H., Shlosman, I., Peletier, R.F. 2000, ApJ, 529, 93

Kormendy, J. 1982, ApJ, 257, 75

Kotilainen, J.K., Reunanen, J., Laine, S.. Ryder, S.D. 2000, A&A, 353, 834

Laine, S., Shlosman, I., Knapen, J.H., Peletier, R.F. 2002, ApJ, 567, 97

Maiolino, R., Alonso-Herrero, A., Anders, S., Quillen, A., Rieke, M.J., Rieke, G.H., Tacconi-Garman, L.E. 2000, ApJ, 531, 219

Martinez-Valpuesta, I., Shlosman, I. 2004, ApJ, 613, L29

Massett, F., Tagger, M. 1997, A&A, 322, 442

Mirabel, I.F., et al. 1999, A&A, 341, 667

Miyamoto, M., Nagai, R. 1975, Publ. Astron. Soc. Japan, 27, 533

Sandage, A., Brucato, R. 1979, AJ, 84, 472

Schwarz, M.P. 1981, ApJ, 247, 77

Shaw, M. A., Axon, D. J., Probst, R., Gatley, I. 1995, MNRAS, 274, 369

Shlosman, I., Frank, J., Begelman, M.C. 1989, Nature, 338, 45

Shlosman, I., Begelman, M.C., Frank, J. 1990, Nature, 345, 679

Shlosman, I., Heller, C.H. 2002, ApJ, 565, 921

Shlosman, I. 2003, in *Active Galactic Nuclei: from Central Engine to Host Galaxy,* eds. S.Collin et al. (ASP Conf. Ser., 290), 427

Stone, J.M. Norman, M.L. 1992, ApJS, 80, 753

Sygnet, J.F., Tagger, M., Athanassoula, E., Pellat, R. 1988, MNRAS, 232, 733

Udry, S., Pfenniger, D. 1988, A&A, 198, 135

Wada, K., Habe, A. 1992, MNRAS, 258, 82

This 2-column preprint was prepared with the AAS LaTeX macros v5.2.